

# Chorus-driven resonant scattering of diffuse auroral electrons in nondipolar magnetic fields

Binbin Ni,<sup>1</sup> Richard M. Thorne,<sup>1</sup> Yuri Y. Shprits,<sup>1,2</sup> Ksenia G. Orlova,<sup>1,3</sup> and Nigel P. Meredith<sup>4</sup>

Received 7 January 2011; revised 8 March 2011; accepted 5 April 2011; published 30 June 2011.

[1] We perform a comprehensive analysis of resonant scattering of diffuse auroral electrons by oblique nightside chorus emissions present along a field line with an equatorial crossing of  $6 R_E$  at 00:00 MLT, using various nondipolar Tsyganenko magnetic field models. Bounce-averaged quasi-linear diffusion coefficients are evaluated for both moderately and actively disturbed geomagnetic conditions using the T89, T96, and T01s models. The results indicate that inclusion of nondipolar magnetic field leads to significant changes in bounce-averaged rates of both pitch angle and momentum diffusion for 200 eV to 10 keV plasma sheet electrons. Compared to the results using a dipole field, the rates of pitch angle diffusion obtained using the Tsyganenko models are enhanced at all resonant pitch angles for 200 eV electrons. In contrast, for 500 eV to 10 keV electrons the rates of pitch angle scattering are enhanced at intermediate and/or high pitch angles but tend to be considerably lower near the loss cone, thus reducing the precipitation loss compared to that in a dipole field. Upper band chorus acts as the dominant cause for scattering loss of 200 eV to 2 keV electrons, while lower band chorus scattering prevails for 5–10 keV electrons, consistent with the results using the dipole model. The first-order cyclotron resonance and the Landau resonance are mainly responsible for the net scattering rates of plasma sheet electrons by oblique chorus waves and also primarily account for the differences in bounce-averaged diffusion coefficients introduced by the use of Tsyganenko models. As the geomagnetic activity increases, the differences in scattering rates compared to the dipole results increase accordingly. Nonnegligible differences also occur particularly at high pitch angles for the diffusion rates between the Tsyganenko models, showing an increase with geomagnetic activity level and a dependence on the discrepancy between the Tsyganenko model fields. The strong dependence of bounce-averaged quasi-linear scattering rates on the adopted global magnetic field model and geomagnetic activity level demonstrates that realistic magnetic field models should be incorporated into future modeling efforts to accurately quantify the role of magnetospheric chorus in driving the diffuse auroral precipitation and the formation of electron pancake distributions.

**Citation:** Ni, B., R. M. Thorne, Y. Y. Shprits, K. G. Orlova, and N. P. Meredith (2011), Chorus-driven resonant scattering of diffuse auroral electrons in nondipolar magnetic fields, *J. Geophys. Res.*, 116, A06225, doi:10.1029/2011JA016453.

## 1. Introduction

[2] It is well established that the diffuse aurora, much weaker than the discrete aurora and generally subvisual with

the naked eye, provides the major source of energy input to the Earth's upper atmosphere at night [e.g., Sandford, 1968; Hardy *et al.*, 1985, 1989; Frahm *et al.*, 1997; Newell *et al.*, 2009, 2010] responsible for the coupling between the magnetosphere and the ionosphere [e.g., Wolf *et al.*, 1991]. Earlier studies suggested that very low frequency (VLF) whistler mode chorus and electrostatic electron cyclotron harmonic (ECH) waves both contribute to diffuse auroral precipitation [e.g., Kennel *et al.*, 1970; Young *et al.*, 1973; Lyons, 1974; Swift, 1981; Belmont *et al.*, 1983; Roeder and Koons, 1989; Inan *et al.*, 1992; Johnstone *et al.*, 1993; Villalón and Burke, 1995; Meredith *et al.*, 1999, 2000, 2009; Horne and Thorne, 2000; Chen and Schulz, 2001a, 2001b; Horne *et al.*, 2003; Ni *et al.*, 2008; Su *et al.*, 2009; Miyoshi *et al.*, 2010]. Assuming

<sup>1</sup>Department of Atmospheric and Oceanic Sciences, University of California, Los Angeles, California, USA.

<sup>2</sup>Institute of Geophysics and Planetary Physics, University of California, Los Angeles, California, USA.

<sup>3</sup>Skobeltsyn Institute of Nuclear Physics, Lomonosov Moscow State University, Moscow, Russia.

<sup>4</sup>British Antarctic Survey, Natural Environment Research Council, Cambridge, UK.

that the scattering process is stochastic, we may quantify the resonant scattering of diffuse auroral electrons (hundreds of eV to tens of keV) by plasma waves in space using a quasi-linear formulism to evaluate pitch angle, momentum, and mixed (pitch angle, momentum) diffusion coefficients [e.g., Lyons, 1974; Horne and Thorne, 2000; Horne et al., 2003; Ni et al., 2008; Su et al., 2009, 2010; Ni et al., 2011a, 2011b]. Recently, Thorne et al. [2010] demonstrated, by a detailed analysis of chorus and ECH waves observed on the CRRES satellite and by using Fokker-Planck diffusion calculations, that scattering by chorus is the dominant cause of the most intense diffuse auroral precipitation, which resolved a long-standing controversy over which wave mode is more important to the production of the diffuse aurora.

[3] To quantify the effect of resonant wave-particle interactions due to quasi-linear diffusion by using the Fokker-Planck equation, bounce averaging of local diffusion coefficients needs to be carried out along the magnetic field line over a particle bounce orbit. Determination of bounce-averaged quasi-linear diffusion coefficients depend on the spectral properties and latitudinal distribution of waves, as well as the background electron density and magnetic field [e.g., Summers, 2005; Thorne et al., 2005; Shprits et al., 2006a; Summers et al., 2007a, 2007b; Albert, 2007; Summers and Ni, 2008; Ni et al., 2008; Shprits and Ni, 2009; Su et al., 2010]. Following Lyons et al. [1972], a dipole magnetic field has usually been adopted to compute bounce-averaged quasi-linear diffusion coefficients. However, during geomagnetically disturbed periods (e.g., magnetic storms and substorms), the realistic ambient magnetic field in the auroral zone ( $L > \sim 5$ ) often deviates considerably from a dipole representation both in configuration and strength. A recent study of Orlova and Shprits [2010] calculated the bounce-averaged pitch angle diffusion rates of 1 MeV electrons due to chorus waves for various distances and two MLTs (00:00 and 12:00) using the Tsyganenko 89 magnetic field model [Tsyganenko, 1989] for  $K_p = 2$  and  $K_p = 6$ . They found that on the dayside the effects of taking a realistic magnetic field into account are negligible at distances less than  $6 R_E$ , but on the nightside diffusion coefficients may depend significantly on the assumed field model. Their results suggest the importance of including a realistic magnetic field in quasi-linear diffusion coefficient computations. However, their analysis was focused on relativistic radiation belt electrons and restricted to a parallel propagation assumption on chorus waves, for which only the first-order cyclotron resonance occurs.

[4] For plasma sheet electrons between hundreds of eV and tens of keV, which form the source population responsible for diffuse auroral precipitation, both the Landau resonance and multiple cyclotron resonances with dual-band oblique chorus emissions (lower band and upper band) play an important role in electron diffusion in energy and pitch angle [Ni et al., 2008, 2011b; Tao et al., 2011]. The diffuse aurora intensity characteristically peaks in the midnight-to-dawn sector [Petrinec et al., 1999; Anderson et al., 2001; Newell et al., 2009, 2010], where both the magnitude and configuration of the background magnetic field is strongly impacted by the intensity of geomagnetic activity. Consequently, this investigation is directed toward quantifying the resonant scattering of diffuse auroral electrons by oblique chorus waves in more realistic, nondipolar magnetic fields.

[5] In the present study, we concentrate on one representative radial distance of  $R_0 = 6 R_E$  at the magnetic equator plane and one specified MLT = 00:00. In section 2 we describe an improved model of two-band chorus emissions, developed by a statistical analysis of CRRES wave observations. Three Tsyganenko magnetic field models are adopted to represent a more realistic ambient magnetic field. Computation of the bounce-averaged diffusion rates for diffuse auroral electrons (200 eV to 10 keV) using the Tsyganenko models and comparison with the results in the dipole field are presented in section 3. We also explore the contribution of various resonance harmonics to driving pitch angle scattering and momentum diffusion of these plasma sheet electrons. We discuss the results in section 4 and finally state our conclusions in section 5.

## 2. Chorus Wave Model and Magnetic Field Models

[6] Following previous studies [e.g., Lyons et al., 1972; Glauert and Horne, 2005; Ni et al., 2008, 2011b; Shprits and Ni, 2009; Su et al., 2009, 2010], we assume that the chorus wave power spectral density  $B^2(f)$  is distributed according to a Gaussian frequency distribution with cutoffs  $f_{lc}$  and  $f_{uc}$ , median value  $f_m$ , and bandwidth  $\delta f$ :

$$B^2(f) = B_W^2 \frac{2}{\sqrt{\pi} \delta f} \left[ \text{erf}\left(\frac{f_m - f_{lc}}{\delta f}\right) + \text{erf}\left(\frac{f_{uc} - f_m}{\delta f}\right) \right]^{-1} \cdot \exp\left[-\left(\frac{f - f_m}{\delta f}\right)^2\right], \quad (1)$$

where  $B_W$  is averaged chorus magnetic field amplitude and  $\text{erf}$  is the error function.

[7] In the present study we concentrate on nightside chorus waves at  $R_0 = 6 R_E$  since the power spectral intensity of chorus waves and the diffuse aurora are strongest around this region [e.g., Petrinec et al., 1999; Meredith et al., 2001, 2009; Li et al., 2009; Newell et al., 2009, 2010] and also the ambient magnetic field can be considerably different from a dipole approximation at this location. The properties of nightside chorus waves at  $R_0 = 6 R_E$  are obtained from a statistical analysis of the magnetic field power spectral densities obtained from the 15 month CRRES wave data set within the 00:00–06:00 MLT sector averaged over the equatorial radial distance range of 5.8–6.2  $R_E$ . As an improvement to the chorus wave model, nightside lower band chorus (LBC:  $0.05 < f/f_{ce} < 0.5$ , where  $f_{ce}$  is equatorial electron gyrofrequency) is averaged over three magnetic latitude intervals of  $| \lambda | \leq 5^\circ$ ,  $5^\circ < | \lambda | \leq 10^\circ$  and  $10^\circ < | \lambda | \leq 15^\circ$  and nightside upper band chorus (UBC:  $0.5 < f/f_{ce} < 0.7$ ) is averaged over two latitude intervals of  $| \lambda | \leq 5^\circ$  and  $5^\circ < | \lambda | \leq 10^\circ$  to take into account the latitudinal dependence of nightside chorus wave power. This investigation also mainly focuses on geomagnetically moderate conditions ( $100 \text{ nT} < AE^* < 300 \text{ nT}$ , where  $AE^*$  is the maximum value of the  $AE$  index in the previous 3 h) which occur during the majority of time period that the diffuse aurora is enhanced. After applying least squares Gaussian fits to the averaged magnetic field intensities as a function of wave frequency normalized to  $f_{ce}$ , the relevant proper-

**Table 1.** Magnetic Field Amplitude  $B_w$ , Peak Wave Frequency  $f_m$ , and Bandwidth  $\Delta f$  Obtained by Applying Gaussian Fits to CRRES Magnetic Field Intensities Averaged Over  $L = 5.8\text{--}6.2$  in the Specified Magnetic Latitude Intervals for Nightside (00:00–06:00 MLT) Lower Band and Upper Band Chorus Under Geomagnetically Moderate Conditions ( $100 \text{ nT} < AE^* < 300 \text{ nT}$ ) and an Empirical Wave Normal Angle Distribution With Latitudinal Dependence Adopted for Lower Band Chorus and Upper Band Chorus Based on Previous Theoretical Simulations and Space-Borne Observations<sup>a</sup>

|                     | LBC (0.05–0.5 $f_{ce}$ ) |                                     |                                      | UBC (0.5–0.7 $f_{ce}$ )  |                                     |
|---------------------|--------------------------|-------------------------------------|--------------------------------------|--------------------------|-------------------------------------|
|                     | $ \lambda  \leq 5^\circ$ | $5^\circ <  \lambda  \leq 10^\circ$ | $10^\circ <  \lambda  \leq 15^\circ$ | $ \lambda  \leq 5^\circ$ | $5^\circ <  \lambda  \leq 10^\circ$ |
| $B_w$ (pT)          | 24.4                     | 56.8                                | 21.1                                 | 20.2                     | 7.4                                 |
| $f_m/f_{ce}$        | 0.36                     | 0.27                                | 0.26                                 | 0.58                     | 0.57                                |
| $\Delta f/f_{ce}$   | 0.09                     | 0.13                                | 0.09                                 | 0.05                     | 0.04                                |
| $\theta_{lc}$ (deg) | 0                        | 0                                   | 0                                    | 0                        | 0                                   |
| $\theta_{uc}$ (deg) | 58                       | 58                                  | 58                                   | 44                       | 44                                  |
| $\theta_m$ (deg)    | 0                        | 30                                  | 50                                   | 0                        | 40                                  |
| $\theta_w$ (deg)    | 30                       | 30                                  | 30                                   | 30                       | 30                                  |

<sup>a</sup>LBC, lower band chorus; UBC, upper band chorus.

ties of nightside chorus wave parameters under moderately disturbed conditions are shown in the top half of Table 1.

[8] The wave normal distribution of chorus emissions is also assumed to be Gaussian and given by

$$g(\theta) = \exp \left[ - \left( \frac{\tan \theta - \tan \theta_m}{\tan \theta_w} \right)^2 \right] (\theta_{lc} \leq \theta \leq \theta_{uc}), \quad (2)$$

where  $\theta$  is wave normal angle,  $\theta_m$  is wave angle with peak power,  $\theta_w$  is the angular width, and  $\theta_{lc}$  and  $\theta_{uc}$  are the lower and upper bounds to the wave normal distribution outside which the wave power is zero. In the present study we use an improved empirical model of the wave normal angle distribution of lower band and upper band chorus, which varies with magnetic latitude, based on previous theoretical simulations and observations [e.g., Thorne and Kennel, 1967; Burton and Holzer, 1974; Goldstein and Tsurutani, 1984; Hayakawa et al., 1984; LeDocq et al., 1998; Hospodarsky et al., 2001; Lauben et al., 2002; Bortnik et al., 2006, 2007; Li et al., 2008; Breneman et al., 2009; Santolik et al., 2009; Haque et al., 2010], and shown in the bottom half of Table 1.

[9] To represent the realistic magnetic field, we choose three Tsyganenko external magnetic field models, T89 [Tsyganenko, 1989], T96 [Tsyganenko and Stern, 1996], and T01s [Tsyganenko et al., 2003] and the IGRF model as the internal magnetic field. While the Tsyganenko magnetic field models are empirical, they assume physical mechanisms embodied by the solar wind inputs and contributions from different current systems, the accuracy of which largely controls the model performance. Compared to the T89 model that only uses  $K_p$  as input and incorporates the contributions of magnetotail warping (due to dipole tilt) and spatial variation of the current sheet, the T96 model uses  $Dst$ , solar wind dynamic pressure  $P_{dyn}$ , and IMF  $B_y$  and  $B_z$  in GSM coordinates as inputs. T96 includes terms from the magnetotail current sheet, ring current, magnetopause current, and terms for Birkeland (field-aligned) currents. As an update to T96, the T01s model considers dawn-dusk asymmetry via inclusion of the partial ring current with field-aligned closure currents. Besides the four input parameters for T96, the T01s model requires two composite parameters (G2 [Tsyganenko, 2002] and G3 [Tsyganenko et al., 2003]) associated with solar wind velocity and interplanetary magnetic field.

[10] In this study we select a group of the above required parameters typical for geomagnetically moderate conditions, that is,  $K_p = 4$ ,  $Dst = -47 \text{ nT}$ ,  $P_{dyn} = 2.6 \text{ nPa}$ , IMF  $B_y = -3.5 \text{ nT}$ , IMF  $B_z = -3.47 \text{ nT}$ , G2 = 4.57, and G3 = 2.33. We use the ONERA-DESP library V4.2 (user's guide available at [http://www.onercert.fr/cratere/support/user\\_guide.html](http://www.onercert.fr/cratere/support/user_guide.html)) to trace the magnetic field line crossing the specific equatorial location and to compute the field values along the entire field line between the two hemispheric footprints. Figure 1 shows the model results of field line configuration (top) in the GSM XZ plane and the magnetic field amplitude along the field line (middle) with  $R_0 = 6 R_E$  at 00:00 MLT, color coded for different magnetic field models. Compared to the dipole field (black dashed), the field line is distorted and the profile of field amplitude exhibits considerable stretching for all three Tsyganenko models. The Tsyganenko magnetic fields are weaker than the dipole field near the equatorial region but become stronger at higher latitudes, as is evident in Figure 1c, a zoom-in plot of latitudinal distribution of magnetic field amplitude within  $|\lambda| \leq 15^\circ$  where nightside chorus emissions are characteristically present. In contrast to the dipole field, there is about a factor of 2 decrease in magnetic field strength near the magnetic equator ( $|\lambda| \leq 3^\circ$ ) and a 20% increase or more for  $12^\circ \leq |\lambda| \leq 15^\circ$ . Among the Tsyganenko models, the T96 (blue solid) model exhibits the most stretched field configuration, while T89 (red solid) and T01s (green solid) present similar model results with small difference in field amplitude at  $|\lambda| \leq 15^\circ$  (Figure 1c).

### 3. Diffuse Auroral Scattering Rates

[11] Following Lyons et al. [1972], the general form for bounce-averaged quasi-linear diffusion coefficients in any ambient magnetic field can be written as

$$\langle D_{\alpha\alpha} \rangle = \frac{1}{\tau_B} \int_0^{\tau_B} D_{\alpha\alpha}(\alpha) \left( \frac{\partial \alpha_{eq}}{\partial \alpha} \right)^2 dt, \quad (3a)$$

$$\langle D_{op} \rangle = \frac{1}{\tau_B} \int_0^{\tau_B} D_{op}(\alpha) \left( \frac{\partial \alpha_{eq}}{\partial \alpha} \right) dt, \quad (3b)$$

$$\langle D_{pp} \rangle = \frac{1}{\tau_B} \int_0^{\tau_B} D_{pp}(\alpha) dt, \quad (3c)$$

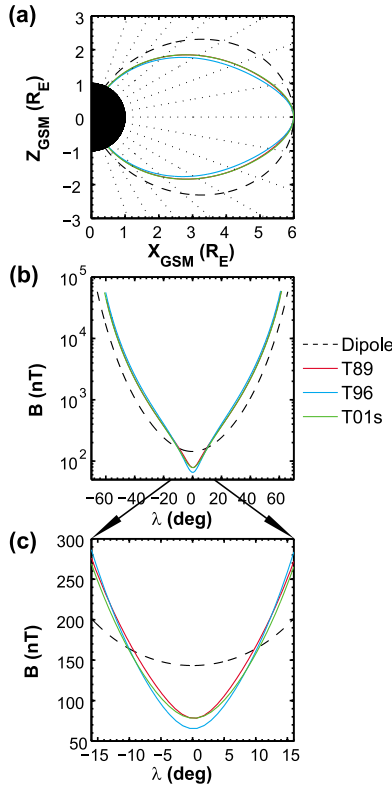


**Figure 1.** Model results of (a) the field line configuration in the GSM XZ plane and (b) the magnetic field strength along the field line with an equatorial crossing of  $6 R_E$  at 00:00 MLT, color coded for the dipole model and three Tsyganenko field models (T89, T96, and T01s). (c) Zoom-in plot of latitudinal distribution of magnetic field amplitude within  $|\lambda| \leq 15^\circ$  where nightside chorus emissions are characteristically present. The dotted lines in Figure 1a denote the constant magnetic latitudes from  $-70^\circ$  to  $70^\circ$  with a step of  $10^\circ$ .

where  $\langle D_{\alpha\alpha} \rangle$ ,  $\langle D_{\alpha p} \rangle$  and  $\langle D_{pp} \rangle$  are bounce-averaged rates of pitch angle diffusion, (pitch angle, momentum) mixed diffusion and momentum diffusion, respectively,  $D_{\alpha\alpha}$ ,  $D_{\alpha p}$  and  $D_{pp}$  are local diffusion coefficients,  $\alpha$  and  $\alpha_{eq}$  are local and equatorial pitch angle, respectively, and  $\tau_B$  is the electron bounce period.

[12] For a dipole field geometry, approximate forms of equations (3a)–(3c) have been derived, and readers are referred to a number of previous studies [e.g., Lyons *et al.*, 1972; Lyons, 1974; Schulz and Lanzerotti, 1974; Glauert and Horne, 2005; Shprits *et al.*, 2006a; Summers *et al.*, 2007a] for details. For nondipolar fields, if the field line lies in a plane perpendicular to the magnetic equator plane, equations (3a)–(3c) can be rewritten as follows [e.g., Orlova and Shprits, 2010]:

$$\langle D_{\alpha\alpha} \rangle = \frac{\int_{\lambda_{m,s}}^{\lambda_{m,n}} \frac{D_{\alpha\alpha}(\alpha)}{\cos \alpha} \left( \frac{\tan \alpha_{eq}}{\tan \alpha} \right)^2 \sqrt{r^2 + \left( \frac{\partial r}{\partial \lambda} \right)^2} d\lambda}{\int_{\lambda_{m,s}}^{\lambda_{m,n}} \sec \alpha \sqrt{r^2 + \left( \frac{\partial r}{\partial \lambda} \right)^2} d\lambda}, \quad (4a)$$

$$\langle D_{\alpha p} \rangle = \frac{\int_{\lambda_{m,s}}^{\lambda_{m,n}} \frac{D_{\alpha p}(\alpha)}{\cos \alpha} \frac{\tan \alpha_{eq}}{\tan \alpha} \sqrt{r^2 + \left( \frac{\partial r}{\partial \lambda} \right)^2} d\lambda}{\int_{\lambda_{m,s}}^{\lambda_{m,n}} \sec \alpha \sqrt{r^2 + \left( \frac{\partial r}{\partial \lambda} \right)^2} d\lambda}, \quad (4b)$$

$$\langle D_{pp} \rangle = \frac{\int_{\lambda_{m,s}}^{\lambda_{m,n}} \frac{D_{pp}(\alpha)}{\cos \alpha} \sqrt{r^2 + \left( \frac{\partial r}{\partial \lambda} \right)^2} d\lambda}{\int_{\lambda_{m,s}}^{\lambda_{m,n}} \sec \alpha \sqrt{r^2 + \left( \frac{\partial r}{\partial \lambda} \right)^2} d\lambda}, \quad (4c)$$

where  $r$  is radial distance to the Earth's center,  $\lambda$  is magnetic latitude, and  $\lambda_{m,s}$  and  $\lambda_{m,n}$  are the mirror latitude of particles on the southern and northern hemisphere, respectively, which are strictly dependent on the field line configuration and the field strength of adopted magnetic field model.

[13] At  $R_0 = 6 R_E$  and 00:00 MLT, the Tsyganenko magnetic field models in GSM coordinates show departure of the field line from  $180^\circ$  magnetic longitude at certain latitudes, i.e., a three-dimensional field line topology. However, the displacement is rather minor, within  $\sim 5^\circ$ , and the difference between the amplitude of the magnetic field along the 3-D field line and the amplitude along the projection of the field line on the GSM XZ plane is very small ( $<\sim 2\%$ ) for any latitude. Therefore, equations (4a)–(4c) are reasonable for the evaluation of bounce-averaged diffusion rates in nondipolar fields.

[14] In this study, we extend the UCLA Full Diffusion Code (FDC) [Ni *et al.*, 2008; Shprits and Ni, 2009], which follows the formulation of Glauert and Horne [2005] and Albert [2007] for quasi-linear local diffusion coefficients ( $D_{\alpha\alpha}$ ,  $D_{\alpha p}$ , and  $D_{pp}$ ), by taking into account the effect of nondipolar magnetic field represented by the Tsyganenko models. Our calculations include contributions from the  $N = -5$  to  $N = 5$  cyclotron harmonic resonances and the Landau resonance  $N = 0$ . The equatorial electron number density at  $R_0 = 6 R_E$  and 00:00 MLT is set as  $6.5 \text{ cm}^{-3}$ , based on the statistically averaged CRRES observations. A constant latitudinal distribution of electron density is adopted following a statistical study of Denton *et al.* [2006], which has showed an only slight change in plasma density below  $\lambda \approx 30^\circ$ .

[15] Figure 2 shows the bounce-averaged pitch angle scattering rates  $\langle D_{\alpha\alpha} \rangle$  as a function of equatorial pitch angle  $\alpha_{eq}$  for plasma sheet electrons at six representative energies from 200 eV to 10 keV, corresponding to the four magnetic field models (color coded with black for dipole field, red for T89, blue for T96, and green for T01s). The pitch angle scattering rates due to nightside LBC ( $0.05\text{--}0.5 f_{ce}$  with  $|\lambda| \leq 15^\circ$ ), UBC ( $0.5\text{--}0.7 f_{ce}$  with  $|\lambda| \leq 10^\circ$ ) and the net scattering rates are shown in the left, middle, and right panels, respectively. There are a number of important features for chorus-driven pitch angle scattering of diffuse auroral electrons in the nondipolar magnetic fields, compared to the results using the dipole model, as follows.

[16] 1. Inclusion of nondipolar magnetic field leads to recognizable changes in the profile of net pitch angle scattering rates for 200 eV to 10 keV electrons. For 200 eV electrons,  $\langle D_{\alpha\alpha} \rangle$  increases by about an order of magnitude in the T96 model and by a factor of  $\sim 5$  in the T89 and T01s models, and also extends to  $\alpha_{eq} > 70^\circ$  where there is an absence of resonance in the dipole field. For 500 eV to 2 keV electrons,  $\langle D_{\alpha\alpha} \rangle$  at low  $\alpha_{eq}$  ( $<\sim 30^\circ$ ) shows a small variation (either a decrease or an increase within a factor of 2) with respect to the three Tsyganenko models, suggestive of a slight influence on the loss time scale of these plasma sheet electrons. However, at higher  $\alpha_{eq}$  ( $>60^\circ$ ) there are pronounced increases in  $\langle D_{\alpha\alpha} \rangle$ , which can produce a more rapid redistribution of 500 eV to 2 keV electrons over pitch angle. For

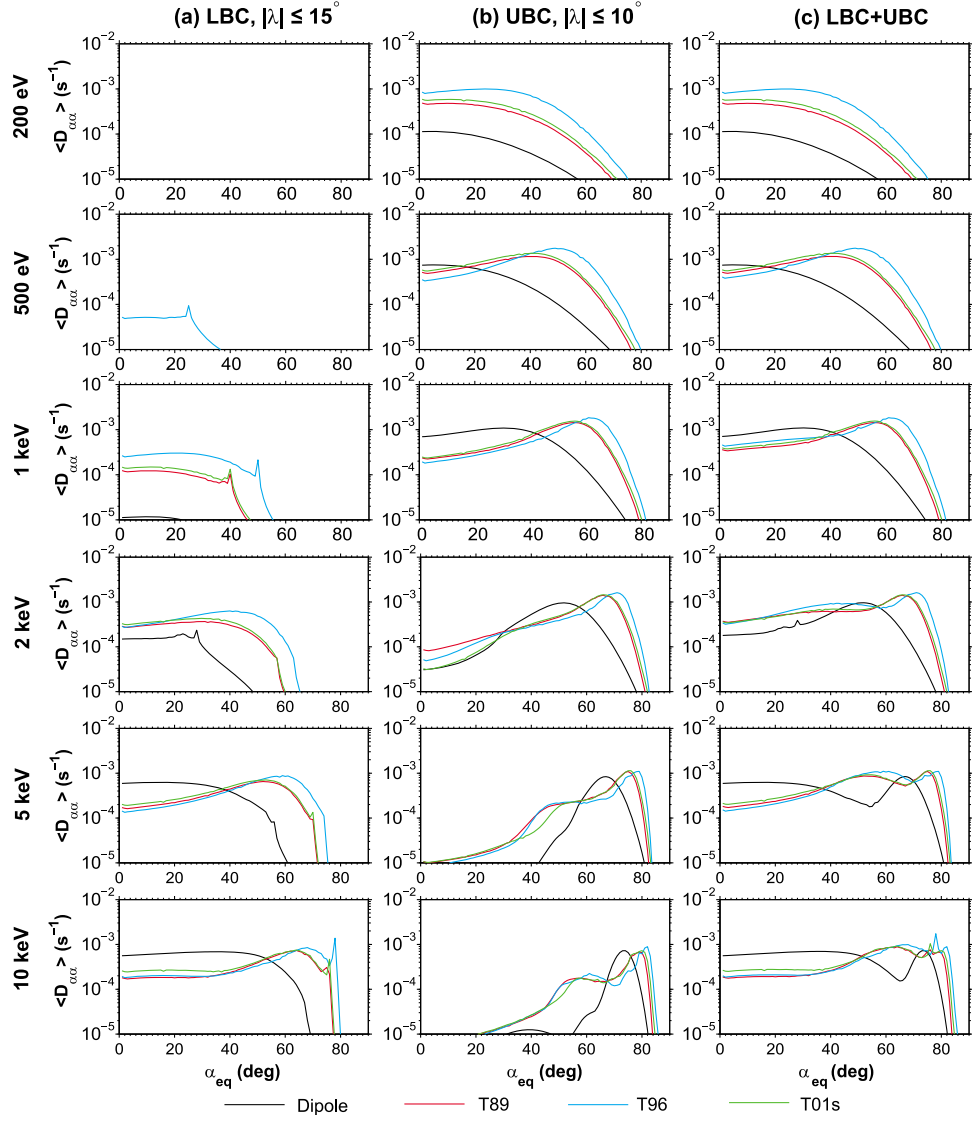


**Figure 2.** Bounce-averaged pitch angle scattering rates  $\langle D_{\alpha\alpha} \rangle$  as a function of equatorial pitch angle  $\alpha_{eq}$  for plasma sheet electrons at six specified energies from 200 eV to 10 keV, color coded with the adopted magnetic field models. Shown are the pitch angle scattering rates due to nightside (left) lower band chorus ( $0.05\text{--}0.5 f_{ce}$  with  $|\lambda| \leq 15^\circ$ ) and (middle) upper band chorus ( $0.5\text{--}0.7 f_{ce}$  with  $|\lambda| \leq 10^\circ$ ) and (right) the net scattering rates.

higher-energy plasma sheet electrons (5–10 keV), pitch angle scattering near the equatorial loss cone becomes less efficient by a factor  $\sim 3$ . Although  $\langle D_{\alpha\alpha} \rangle$  at higher  $\alpha_{eq}$  becomes larger than the dipole model results, the increases show a tendency to flatten the scattering rates at intermediate pitch angles and allow scattering at  $\alpha_{eq}$  closer to  $90^\circ$ . All these variations in pitch angle scattering rates can affect the evolution of the plasma sheet electron pitch angle distribution and the formation of pancake distributions peaked at  $90^\circ$  pitch angles [Wrenn et al., 1979; Meredith et al., 1999, 2000; Li et al., 2010; Tao et al., 2011].

[17] 2. Use of the T96 model field produces the most noticeable difference in pitch angle scattering rates, while the changes in the  $\langle D_{\alpha\alpha} \rangle$  profile are relatively smaller and quite similar for T89 and T01s. This is consistent with the

relative difference of the three Tsyganenko models in the traced field line and modeled field amplitude with respect to the ideal dipole field, as shown in Figure 1. As a consequence, computation of bounce-averaged diffusion coefficients is field model dependent, with the accuracy of diffusion rates closely related to the adopted magnetic field model, the discussion of which will be deferred to section 4.

[18] 3. At low  $\alpha_{eq}$ , LBC-driven scattering rates increase substantially for 200 eV to 1 keV electrons in the Tsyganenko models, become comparable to the dipole model results for 2 keV, and decrease appreciably for 5–10 keV electrons. UBC also causes enhanced scattering of 200 eV electrons in the nondipolar fields, but UBC induced diffusion decreases the scattering rates near the loss cone of 500 eV to 1 keV electrons and increases the precipitation loss of 2–10 keV

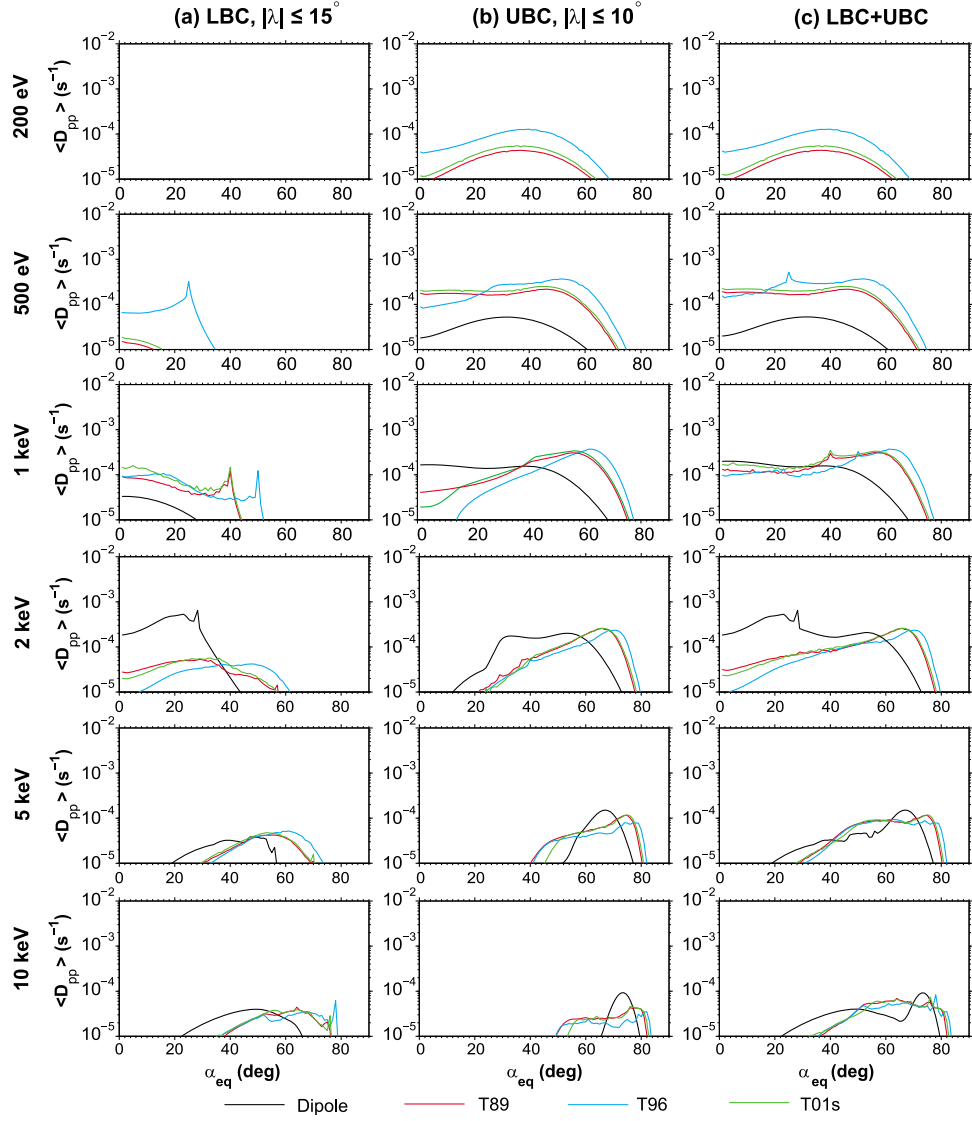


**Figure 3.** Same as in Figure 2 but for bounce-averaged momentum diffusion rates  $\langle D_{pp} \rangle$ .

electrons. At high  $\alpha_{eq}$  close to  $90^\circ$ , both LBC and UBC scattering rates, if present, show substantial increase in the Tsyganenko magnetic fields. In principle, UBC acts as the dominant cause for precipitation loss of 200 eV to 2 keV electrons and LBC plays the major role for pitch angle scattering 5–10 keV electrons, consistent with the previous studies [Ni et al., 2008, 2011b].

[19] The corresponding bounce-averaged momentum diffusion rates  $\langle D_{pp} \rangle$  are shown in Figure 3. The  $\langle D_{pp} \rangle$  profile generally exhibits variations with respect to adopted global magnetic field model in a manner similar to that of  $\langle D_{aa} \rangle$ . Specifically, (1) the most pronounced changes in diffusion rate occur at energies  $<\sim 2$  keV and less noticeable changes at energies  $>\sim 5$  keV, (2) chorus scattering extends to high  $\alpha_{eq}$  closer to  $90^\circ$ , and (3) LBC and UBC play distinct roles in driving resonant diffusion of plasma sheet electron with a pronounced dependence on energy and equatorial pitch angle. For 200–500 eV electrons, the increases in  $\langle D_{pp} \rangle$  for the three Tsyganenko models are sig-

nificant, about an order of magnitude for all resonant  $\alpha_{eq}$  compared to the dipole field results, and also extend to higher  $\alpha_{eq}$ . For 1 and 2 keV electrons, pronounced increase in  $\langle D_{pp} \rangle$  occurs at  $\alpha_{eq} \approx 70^\circ$  while  $\langle D_{pp} \rangle$  at low  $\alpha_{eq}$  shows small changes for 1 keV electrons and decreases by a factor of 5 or more for 2 keV electrons. For 5–10 keV electrons, there is small difference in momentum diffusion rates except that the resonant scattering occurs at high  $\alpha_{eq}$  closer to  $90^\circ$  in the nondipolar fields, which can induce enhanced acceleration of these plasma sheet electrons. Similar to the results for pitch angle scattering, calculations with T96 model produce the largest difference in momentum diffusion, in particular for  $\leq 5$  keV electrons, when compared to the dipole model results.

[20] Figure 4 illustrates how different resonance harmonics contribute to the chorus-driven pitch angle scattering rates in different global magnetic field models. Only the results for five resonance harmonics with  $|N| \leq 2$  are shown because the roles of the other higher-order resonances are

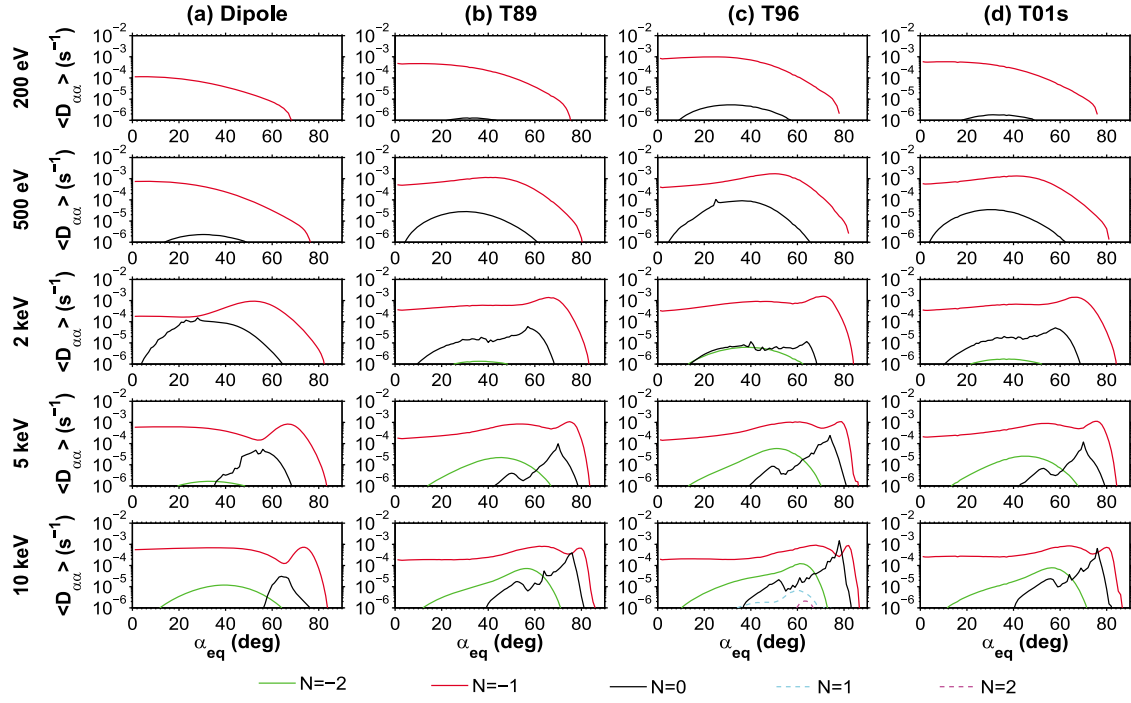


**Figure 4.** Bounce-averaged pitch angle scattering rates of different resonance harmonics ( $|N| \leq 2$ ) for plasma sheet electrons at the indicated five energies from 200 eV to 10 keV, using (a) the dipole model, (b) T89, (c) T96, and (d) T01s.

comparatively negligible. The first-order cyclotron resonance ( $N = -1$ ) always plays the dominant role in pitch angle scattering of diffuse auroral electrons, and the Landau resonance ( $N = 0$ ) becomes important at intermediate and high equatorial pitch angles with an energy dependence.

$N = -2$  cyclotron resonance also plays a role in scattering 2–10 keV electrons, but higher-order cyclotron resonances  $N = 1$  and 2 only cause scattering of 10 keV electrons in the T96 field and their relative contributions are quite minor. As a consequence, differences in the net rates of  $\langle D_{\alpha\alpha} \rangle$  for

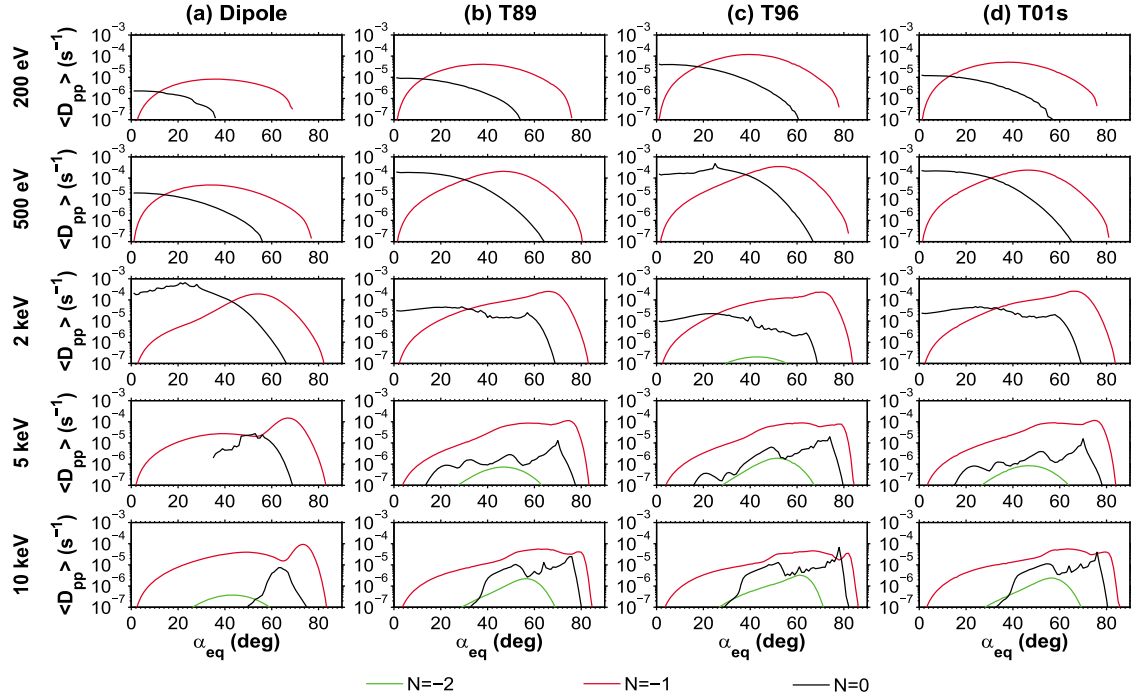


**Figure 5.** Same as in Figure 4 but for bounce-averaged momentum diffusion rates  $\langle D_{pp} \rangle$ .

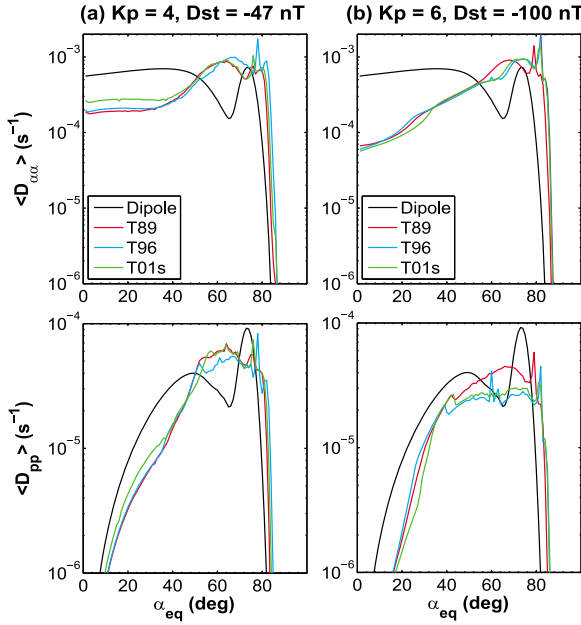


**Figure 6.** Comparison of  $\langle D_{\alpha\alpha} \rangle$  and  $\langle D_{pp} \rangle$  by nightside chorus for 10 keV electrons using the indicated four magnetic field models for two representative geomagnetic activity conditions: (a) moderately disturbed conditions with  $K_p = 4$  and  $Dst = -47$  nT and (b) actively disturbed conditions with  $K_p = 6$  and  $Dst = -100$  nT.

use of the Tsyganenko fields are mainly attributed to changes in the first-order cyclotron resonance and Landau resonance scattering rates. We also note that the variation in  $\langle D_{\alpha\alpha} \rangle$  at low  $\alpha_{eq}$  is mainly attributed to the first-order resonance, which controls the loss time scales of plasma sheet electrons that are approximately inversely proportional to  $\langle D_{\alpha\alpha} \rangle$  near the edge of equatorial loss cone [Shprits et al., 2006b; Albert and Shprits, 2009]. At intermediate and high  $\alpha_{eq}$ , the variation in  $\langle D_{\alpha\alpha} \rangle$  is mainly due to a combined effect of the first-order cyclotron resonance and Landau resonance, with an additional contribution from  $N = -2$  cyclotron resonance particularly for 5–10 keV electrons.

[21] For the five energies from 200 eV to 10 keV, bounce-averaged momentum diffusion rates  $\langle D_{pp} \rangle$  for resonance harmonics  $N = -2, -1$ , and 0 are presented in Figure 5, from left to right, for the dipole model and three Tsyganenko models, T89, T96 and T01s. The results of the other higher-order resonance harmonics are not shown, owing to their substantially minor contributions in comparison. In contrast to the results for  $\langle D_{\alpha\alpha} \rangle$ , the Landau resonance dominates over the first-order cyclotron resonance (by several orders of magnitude) to account for the net momentum diffusion and its variation at low  $\alpha_{eq}$  for 200 eV to 2 keV electrons, demonstrating the importance of Landau resonance in redistributing these electrons over energy space and modifying the energy transfer between the electrons and the waves. For 5 and 10 keV electrons at low  $\alpha_{eq}$ , the first-order cyclotron resonance becomes dominantly responsible for the changes in  $\langle D_{pp} \rangle$  introduced by use of nondipolar fields, but the Landau resonance scattering is negligible compared to that for 200 eV to 2 keV electrons. For intermediate  $\alpha_{eq}$  both

first-order cyclotron resonance and Landau resonance compete in the momentum diffusion of plasma sheet electrons, while at high  $\alpha_{eq}$  the first-order cyclotron resonance scattering is always most efficient and the effect of Landau resonance becomes comparable only for high-energy electrons.  $N = -2$  resonance plays a modest role for 5–10 keV electrons, similar to that for  $\langle D_{\alpha\alpha} \rangle$ .

[22] To examine the dependence of chorus-driven diffuse auroral scattering rates on geomagnetic activity level, Figure 6, as an example, shows the comparative results of  $\langle D_{\alpha\alpha} \rangle$  (upper panels) and  $\langle D_{pp} \rangle$  (lower panels) for 10 keV electrons at  $R_0 = 6 R_E$  and MLT = 00:00 for the representative conditions for two geomagnetic activity levels, that is, for geomagnetically moderate conditions (left panels) with  $K_p = 4$ ,  $Dst = -47$  nT,  $P_{dyn} = 2.6$  nPa, IMF  $B_y = -3.5$  nT, IMF  $B_z = -3.47$  nT, G2 = 4.57, and G3 = 2.33, and for geomagnetically active conditions (right panels) with  $K_p = 6$ ,  $Dst = -100$  nT,  $P_{dyn} = 4.8$  nPa, IMF  $B_y = 5$  nT, IMF  $B_z = -6$  nT, G2 = 19, and G3 = 18. To extract the major effect of magnetic field variations under different geomagnetic conditions and to minimize the influence of other factors such as the variations in wave power and electron density, we have chosen the same nightside chorus spectral distribution, its latitudinal extent and ambient electron density as those for moderate conditions to compute the scattering rates for active conditions. Apparently, as the geomagnetic activity intensifies, the differences in computed scattering rates (both  $\langle D_{\alpha\alpha} \rangle$  and  $\langle D_{pp} \rangle$ ) between the dipole and nondipolar fields increase accordingly, which is primarily due to the increased deviation of Tsyganenko model results from the dipole field during active times and also further demonstrates the importance of using realistic magnetic field models to quantifying resonant scattering of magnetospheric electrons by plasma waves. Although the differences in scattering rates between the Tsyganenko models are not significant, there are nonnegligible changes particularly at high  $\alpha_{eq}$  that increase with geomagnetic activity level and depend on the discrepancy between the Tsyganenko model fields.

#### 4. Discussion

[23] Variations in  $\langle D_{\alpha\alpha} \rangle$ ,  $\langle D_{pp} \rangle$  and  $\langle D_{op} \rangle$  (not shown) introduced by use of Tsyganenko field models will affect the redistribution of plasma sheet electrons over energy and pitch angle as well as cause a change in the MLT dependence of diffuse auroral precipitation. For instance, for hundreds of eV electrons, the precipitation becomes more efficient as a result of enhanced pitch angle scattering near the edge of loss cone in the Tsyganenko models so that these electrons cannot travel far following the injection on the nightside. In contrast, the loss time scales of higher-energy electrons (5–10 keV) increase by a factor of  $\sim 3$  in the Tsyganenko models, demonstrating a slower loss to the atmosphere and an increased possibility of transport to the dayside in the nondipolar fields. In addition, extension of resonant diffusion of diffuse auroral electrons to high  $\alpha_{eq}$  closer to 90°, together with an increase in both  $\langle D_{\alpha\alpha} \rangle$  and  $\langle D_{pp} \rangle$  at high  $\alpha_{eq}$ , suggests that the trapped electron population will be subject to enhanced acceleration and pitch angle scattering in the nondipolar fields.

[24] Figures 4 and 5 clearly show that chorus-associated diffuse auroral precipitation mainly results from the first-

order cyclotron resonance and Landau resonance, regardless of the adopted magnetic field model. The first-order cyclotron resonance plays the most important role in pitch angle scattering, but for momentum diffusion the first-order cyclotron resonance dominates only at intermediate and high  $\alpha_{eq}$  while the Landau resonance prevails at low  $\alpha_{eq}$ . Under most circumstances, higher-order cyclotron resonances make insignificant contributions to the diffuse auroral precipitation. However, the  $N = -2$  resonance scattering can be comparable to the Landau resonance scattering for 5–10 keV electrons at intermediate  $\alpha_{eq}$ . Therefore, inclusion of oblique propagation of chorus waves is essential to quantify chorus-driven diffuse auroral scattering. Variations in bounce-averaged diffusion rates associated with the first-order cyclotron resonance and Landau resonances are also responsible for the changes in the net diffuse auroral scattering by oblique chorus in more realistic magnetic fields. As pointed out by *Orlova and Shprits* [2010], changes in magnetic field strength along the field line alter the wave dispersion relation and the wave-particle resonance condition so that electrons can resonate with the waves for the same equatorial pitch angle at lower latitudes on the nightside for the Tsyganenko field model than in the dipole field. We also note that decrease in magnetic field strength near the equatorial region in the Tsyganenko models (Figure 1c) lowers the minimum resonant energy of electrons interacting with chorus waves [e.g., *Summers et al.*, 2007a; *Orlova and Shprits*, 2010], which can explain the pronounced increase in scattering rates of 200 eV electrons for which resonance only occurs near the equator. In addition, changes in field line configuration can lead to changes in electron bounce period, which also contributes to the difference in bounce-averaged diffusion coefficients using nondipolar fields.

[25] As a result of similarity in the traced field line and modeled field amplitude, use of T89 and T01s tends to exhibit noticeable but similar differences in bounce-averaged diffusion rates, compared to the dipole field results. Use of T96 introduces the largest difference in net diffusion rates, as shown in Figures 2 and 3. The dependence of quasi-linear scattering rates on the adopted global magnetic field model demonstrates that accurate evaluations of bounce-averaged diffusion coefficients rely closely on the ability of adopted magnetic field model to represent the field strength and configuration of ambient magnetic field. *Chen et al.* [2006] explored the uncertainties associated with a number of empirical external magnetic field models by applying a best fitting method to multipoint magnetic field measurements. They demonstrated that for quiescent times with  $-30 \text{ nT} < Dst < 50 \text{ nT}$ , several models including T01s compete with each other and have similar performance, all with reasonably low error percentages. However, for storm periods with  $-180 \text{ nT} < Dst < -30 \text{ nT}$ , T01s has an outstanding performance and the largest chance (typically 60–80%) of providing the best fits to the measurements. *McCollough et al.* [2008] also quantitatively examined the accuracy of Tsyganenko field models, using magnetic field data for 2 years (1996 and 2003) characterized by very different space weather conditions. They found that while T96 is a very popular model and performs better than the basic models, it is likely significantly overstretched and should be replaced by T01s under geomagnetically disturbed

conditions. These investigations suggest a preference of using T01s to model the ambient magnetic field for a most reliable quantification of bounce-averaged diffuse auroral scattering rates, mainly due to its comparatively better performance under most geomagnetic conditions.

[26] In this study we have mainly focused on a representative moderately disturbed geomagnetic condition ( $Kp = 4$  and  $Dst = -47 \text{ nT}$ ) with  $R_0 = 6 R_E$  at MLT = 00:00 since both the diffuse aurora activity and chorus emissions are commonly most intense around this region. We have also performed a comparative analysis of chorus-driven diffuse auroral scattering rates using different magnetic field models for moderately and actively disturbed conditions (Figure 6). Not surprisingly, besides the geomagnetic activity dependence, the effect of nondipolar magnetic field on chorus-driven diffuse auroral scattering depends on L shell and MLT, which will be left for our following studies to establish a more accurate diffuse auroral scattering model as a function of L shell, MLT, electron energy, and geomagnetic activity using realistic magnetic field models and improved chorus wave information. However, a number of general comments can be presented here. Since the ambient magnetic field on the nightside ( $\sim 20:00\text{--}04:00$  MLT) is much more likely to be distorted than on the dayside, we anticipate a much smaller impact of the realistic dayside magnetic field on chorus-driven scattering loss of plasma sheet electrons as they drift toward the dawn sector onto the dayside. We note that *Orlova and Shprits* [2010] demonstrated that the scattering of radiation belt relativistic electrons on the dayside, taking into account a more realistic magnetic field, yielded negligible differences from that in a dipole field at distances  $\leq 6 R_E$ . Also the nightside field line configuration and magnetic field strength is close to a dipole topology at L shells  $< 4$  during geomagnetically quiet times, while the magnetic field becomes more stretched under actively disturbed conditions at higher L shells. Consequently it is expected that the effect of nondipolar magnetic field on diffuse auroral precipitation should become more significant at higher L shells when geomagnetic activity intensifies. For geomagnetically disturbed cases, the increased deviation of realistic magnetic field from a dipole field can enhance the modification of the resonant wave-particle interaction process and the resultant scattering rates. In addition, intense chorus emissions with extremely large amplitude [e.g., *Cattell et al.*, 2008; *Cully et al.*, 2008] are more likely to occur; therefore, nonlinear diffusion by extremely intense chorus [e.g., *Bortnik et al.*, 2008] in the realistic ambient magnetic field also tends to play an important role in the diffuse auroral scattering process besides quasi-linear diffusion.

[27] To quantify the quasi-linear bounce-averaged diffuse auroral scattering coefficients, we have developed an improved moderate time, nightside chorus wave model at  $L = 6$  that includes the latitudinal wave power distributions of LBC and UBC, based on a statistical analysis of the entire CRRES wave data. Following *Meredith et al.* [2009], the L value and magnetic latitude were determined using the Olson-Pfizer tilt-dependent static model [Olson and Pfizer, 1977] and the IGRF 85 model. In reality, adoption of different magnetic field models can introduce changes in the determination of L value and magnetic latitude, the extent of which strongly depends on the level

of geomagnetic activity, and thus may affect the statistical distribution of nightside chorus. While the global model of chorus distribution obtained using the CRRES wave measurements (within  $\sim 7 R_E$ ) is much less sensitive to magnetic field models under geomagnetically quiet and moderate conditions, intense geomagnetic disturbances can cause nonnegligible variations in chorus distribution using different magnetic field models and also enhance the effect of nonlinear wave-particle interactions, which need to be carefully addressed in future investigations. Additionally, we have adopted the wave magnetic field spectral intensities converted from the CRRES observed wave electric field spectral intensities under the assumption of parallel propagation [e.g., *Meredith et al.*, 2003] to establish the Gaussian frequency spectrum of LBC and UBC as a function of wave frequency normalized to equatorial electron gyrofrequency. However, there remains unresolved controversy over the wave normal angle distribution of chorus emissions, showing that both LBC and UBC can propagate at various wave normal angles that cover a broad range from field aligned to highly oblique [e.g., *Thorne and Kennel*, 1967; *Hayakawa et al.*, 1984; *Hospodarsky et al.*, 2001; *Lauben et al.*, 2002; *Breneman et al.*, 2009; *Santolik et al.*, 2009; *Haque et al.*, 2010], which subsequently modifies the conversion of electric field spectral intensity to magnetic field spectral intensity and consequently influences the quantification of chorus-driven diffuse auroral scattering rates. We investigate the effect of chorus wave normal angle distribution on the diffuse auroral precipitation in a companion paper (B. Ni et al., Diffuse auroral scattering by whistler mode chorus waves: Dependence on wave normal angle distribution, submitted to *Journal of Geophysical Research*, 2011).

## 5. Conclusions

[28] We have used the Tsyganenko models (T89, T96, and T01s), which are expected to yield a more realistic ambient magnetic field, to quantify chorus-driven resonant diffusion of plasma sheet electrons in the inner magnetosphere under a representative geomagnetically moderate condition. We have also performed a quantitative comparison of computed bounce-averaged diffusion coefficients in the nondipolar fields with the results obtained using the dipole model. Our main conclusions are summarized as follows.

[29] 1. Inclusion of nondipolar magnetic field leads to significant changes in bounce-averaged pitch angle and momentum diffusion rates for 200 eV to 10 keV plasma sheet electrons, the extent of which largely depends on energy, equatorial pitch angle, and adoption of global magnetic field model.

[30] 2. Pitch angle scattering rates increase dramatically in a nondipolar field for 200 eV electrons but tend to decrease by a factor of  $\sim 3$  near the loss cone for 5–10 keV, thereby affecting the loss time scales of diffuse auroral electrons. Energy diffusion increases considerably at high  $\alpha_{eq}$  for 200 eV to 10 keV electrons but decreases at low  $\alpha_{eq}$  for 500 eV to 2 keV electrons. Use of nondipolar fields also extends chorus scattering to high  $\alpha_{eq}$  closer to 90°, which can lead to an enhanced “seed” electron population for subsequent acceleration to radiation belt energies ( $>100$  keV).

[31] 3. Both LBC and UBC scattering rates show substantial changes in the Tsyganenko magnetic fields, compared to the dipole field results. UBC acts as the dominant cause for scattering loss of 200 eV to 2 keV electrons and LBC scattering prevails for 5–10 keV electrons, consistent with the results for a dipole model [*Ni et al.*, 2008, 2011b].

[32] 4. The first-order cyclotron resonance and Landau resonance are mainly responsible for the resonant diffusion of plasma sheet electrons by oblique chorus waves. These two resonances also primarily account for the differences in bounce-averaged diffusion coefficients introduced by the use of Tsyganenko models.

[33] 5. For pitch angle scattering, the first-order cyclotron resonance always plays the major role, and the Landau resonance becomes important only at intermediate and high  $\alpha_{eq}$ , dependent on energy. For momentum diffusion, the Landau resonance dominantly accounts for the net rates and their variation at low  $\alpha_{eq}$  for 200 eV to 2 keV electrons, while the first-order cyclotron resonance prevails at higher pitch angles for the diffuse auroral electrons. These features occur regardless of the adopted magnetic field model.

[34] 6. As the geomagnetic activity increases, the differences in computed scattering rates compared to the dipole results increase accordingly, as a consequence of the increased deviation of adopted magnetic field model from the dipole field. Nonnegligible differences also occur particularly at high  $\alpha_{eq}$  for the diffusion rates between the Tsyganenko models, showing an increase with geomagnetic activity level and a dependence on the discrepancy between the Tsyganenko model fields.

[35] Our study clearly demonstrates that inclusion of realistic magnetic field is essential for accurate quantification of the role of magnetospheric chorus in driving the diffuse auroral precipitation and the formation of electron pancake distributions. Use of bounce-averaged scattering rates in more realistic nondipolar fields for Fokker-Planck diffusion simulations can undoubtedly contribute significantly to more accurate magnetospheric state-based modeling of the global distribution of the diffuse aurora and the evolution of plasma sheet electrons that act as both the source population for the excitation of a number of magnetospheric waves and the seed population for the radiation belt energetic electrons.

[36] **Acknowledgments.** This research was supported by NSF grant ATM-0802843 and NASA grant NNX09AF51G. The authors thank the developers of ONERA-DESP library, including D. Boscher, S. Bourdarie, T. P. O’Brien, and T. Guild.

[37] Masaki Fujimoto thanks George Hospodarsky and another reviewer for their assistance in evaluating this paper.

## References

- Albert, J. M. (2007), Simple approximations of quasi-linear diffusion coefficients, *J. Geophys. Res.*, 112, A12202, doi:10.1029/2007JA012551.
- Albert, J. M., and Y. Y. Shprits (2009), Estimates of lifetimes against pitch angle diffusion, *J. Atmos. Sol. Terr. Phys.*, 71, 1647–1652, doi:10.1016/j.jastp.2008.07.004.
- Anderson, P. C., S. M. Petrinec, and K. Liou (2001), Statistical patterns in X-ray and UV auroral emissions and energetic electron precipitation, *J. Geophys. Res.*, 106(A4), 5907–5911, doi:10.1029/2000JA003041.
- Belmont, G., D. Fontaine, and P. Canu (1983), Are equatorial electron cyclotron waves responsible for diffuse auroral electron precipitation?, *J. Geophys. Res.*, 88(A11), 9163–9170, doi:10.1029/JA088iA11p09163.

- Bortnik, J., U. S. Inan, and T. F. Bell (2006), Landau damping and resultant unidirectional propagation of chorus waves, *Geophys. Res. Lett.*, **33**, L03102, doi:10.1029/2005GL024553.
- Bortnik, J., R. M. Thorne, and N. P. Meredith (2007), Modeling the propagation characteristics of chorus using CRRES suprathermal electron fluxes, *J. Geophys. Res.*, **112**, A08204, doi:10.1029/2006JA012237.
- Bortnik, J., R. M. Thorne, and U. S. Inan (2008), Nonlinear interaction of energetic electrons with large amplitude chorus, *Geophys. Res. Lett.*, **35**, L21102, doi:10.1029/2008GL035500.
- Breneman, A. W., C. A. Kletzing, J. Pickett, J. Chum, and O. Santolik (2009), Statistics of multispacraft observations of chorus dispersion and source location, *J. Geophys. Res.*, **114**, A06202, doi:10.1029/2008JA013549.
- Burton, R., and R. Holzer (1974), The origin and propagation of chorus in the outer magnetosphere, *J. Geophys. Res.*, **79**(7), 1014–1023, doi:10.1029/JA079i007p01014.
- Cattell, C., et al. (2008), Discovery of very large amplitude whistler-mode waves in Earth's radiation belts, *Geophys. Res. Lett.*, **35**, L01105, doi:10.1029/2007GL032009.
- Chen, M., and M. Schulz (2001a), Simulations of storm time diffuse aurora with plasmashell electrons in strong pitch angle diffusion, *J. Geophys. Res.*, **106**(A2), 1873–1886, doi:10.1029/2000JA000161.
- Chen, M., and M. Schulz (2001b), Simulations of diffuse aurora with plasma sheet electrons in pitch angle diffusion less than everywhere strong, *J. Geophys. Res.*, **106**(A12), 28,949–28,966, doi:10.1029/2001JA000138.
- Chen, Y., R. H. W. Friedel, and G. D. Reeves (2006), Phase space density distributions of energetic electrons in the outer radiation belt during two Geospace Environment Modeling Inner Magnetosphere/Storms selected storms, *J. Geophys. Res.*, **111**, A11S04, doi:10.1029/2006JA011703.
- Cully, C. M., J. W. Bonnell, and R. E. Ergun (2008), THEMIS observations of long-lived regions of large-amplitude whistler waves in the inner magnetosphere, *Geophys. Res. Lett.*, **35**, L17S16, doi:10.1029/2008GL033643.
- Denton, R. E., K. Takahashi, I. A. Galkin, P. A. Nsumei, X. Huang, B. W. Reinisch, R. R. Anderson, M. K. Sleeper, and W. J. Hughes (2006), Distribution of density along magnetospheric field lines, *J. Geophys. Res.*, **111**, A04213, doi:10.1029/2005JA011414.
- Frahm, R. A., J. D. Winningham, J. R. Sharber, R. Link, G. Crowley, E. E. Gaines, D. L. Chenette, B. J. Anderson, and T. A. Poterma (1997), The diffuse aurora: A significant source of ionization in the middle atmosphere, *J. Geophys. Res.*, **102**(D23), 28,203–28,214, doi:10.1029/97JD02430.
- Glauert, S. A., and R. B. Horne (2005), Calculation of pitch-angle and energy diffusion coefficients with the PADIE code, *J. Geophys. Res.*, **110**, A04206, doi:10.1029/2004JA010851.
- Goldstein, B., and B. Tsurutani (1984), Wave normal directions of chorus near the equatorial source region, *J. Geophys. Res.*, **89**(A5), 2789–2810, doi:10.1029/JA089iA05p02789.
- Haque, N., M. Spasojevic, O. Santolik, and U. S. Inan (2010), Wave normal angles of magnetospheric chorus emissions observed on the Polar spacecraft, *J. Geophys. Res.*, **115**, A00F07, doi:10.1029/2009JA014717.
- Hardy, D. A., M. S. Gussenhoven, and E. Holeman (1985), A statistical model of auroral electron precipitation, *J. Geophys. Res.*, **90**(A5), 4229–4248, doi:10.1029/JA090iA05p04229.
- Hardy, D. A., M. S. Gussenhoven, and D. Brautigam (1989), A statistical model of auroral ion precipitation, *J. Geophys. Res.*, **94**(A1), 370–392, doi:10.1029/JA094iA01p00370.
- Hayakawa, M., Y. Yamanaka, M. Parrot, and F. Lefevre (1984), The wave normals of magnetospheric chorus emissions observed on board GEOS 2, *J. Geophys. Res.*, **89**(A5), 2811–2821, doi:10.1029/JA089iA05p02811.
- Horne, R. B., and R. M. Thorne (2000), Electron pitch-angle diffusion by electrostatic electron cyclotron harmonic waves: The origin of pancake distributions, *J. Geophys. Res.*, **105**(A3), 5391–5402, doi:10.1029/1999JA900447.
- Horne, R. B., R. M. Thorne, N. P. Meredith, and R. R. Anderson (2003), Diffuse auroral electron scattering by electron cyclotron harmonic and whistler mode waves during an isolated substorm, *J. Geophys. Res.*, **108**(A7), 1290, doi:10.1029/2002JA009736.
- Hospodarsky, G., T. Averkamp, W. Kurth, D. Gurnett, M. Dougherty, U. Inan, and T. Wood (2001), Wave normal and Poynting vector calculations using the Cassini radio and plasma wave instrument, *J. Geophys. Res.*, **106**(A12), 30,253–30,269.
- Inan, U. S., Y. T. Chiu, and G. T. Davidson (1992), Whistler-mode chorus and morningside aurorae, *Geophys. Res. Lett.*, **19**(7), 653–656, doi:10.1029/92GL00402.
- Johnstone, A., D. Walton, R. Liu, and D. Hardy (1993), Pitch angle diffusion of low-energy electrons by whistler mode waves, *J. Geophys. Res.*, **98**(A4), 5959–5967.
- Kennel, C. F., F. L. Scarf, R. W. Fredricks, J. H. McGehee, and F. V. Coroniti (1970), VLF electric field observations in the magnetosphere, *J. Geophys. Res.*, **75**(31), 6136–6152, doi:10.1029/JA075i031p06136.
- Lauben, D. S., U. S. Inan, T. F. Bell, and D. A. Gurnett (2002), Source characteristics of ELF/VLF chorus, *J. Geophys. Res.*, **107**(A12), 1429, doi:10.1029/2000JA003019.
- LeDocq, M. J., D. A. Gurnett, and G. B. Hospodarsky (1998), Chorus source locations from VLF Poynting flux measurements with the Polar spacecraft, *Geophys. Res. Lett.*, **25**(21), 4063–4066, doi:10.1029/1998GL900071.
- Li, W., R. M. Thorne, N. P. Meredith, R. B. Horne, J. Bortnik, Y. Y. Shprits, and B. Ni (2008), Evaluation of whistler mode chorus amplification during an injection event observed on CRRES, *J. Geophys. Res.*, **113**, A09210, doi:10.1029/2008JA013129.
- Li, W., et al. (2009), Global distribution of whistler-mode chorus waves observed on the THEMIS spacecraft, *Geophys. Res. Lett.*, **36**, L09104, doi:10.1029/2009GL037595.
- Li, W., et al. (2010), THEMIS analysis of observed equatorial electron distributions responsible for the chorus excitation, *J. Geophys. Res.*, **115**, A00F11, doi:10.1029/2009JA014845.
- Lyons, L. R. (1974), Electron diffusion driven by magnetospheric electrostatic waves, *J. Geophys. Res.*, **79**(4), 575–580, doi:10.1029/JA079i004p00575.
- Lyons, L. R., R. M. Thorne, and C. F. Kennel (1972), Pitch-angle diffusion of radiation belt electrons within the plasmasphere, *J. Geophys. Res.*, **77**(19), 3455–3474, doi:10.1029/JA077i019p03455.
- McCollough, J. P., J. L. Gannon, D. N. Baker, and M. Gehmeyr (2008), A statistical comparison of commonly used external magnetic field models, *Space Weather*, **6**, S10001, doi:10.1029/2008SW000391.
- Meredith, N. P., A. D. Johnstone, S. Szita, R. B. Horne, and R. R. Anderson (1999), “Pancake” electron distributions in the outer radiation belts, *J. Geophys. Res.*, **104**(A6), 12,431–12,444, doi:10.1029/1998JA900083.
- Meredith, N. P., R. B. Horne, A. D. Johnstone, and R. R. Anderson (2000), The temporal evolution of electron distributions and associated wave activity following substorm injections in the inner magnetosphere, *J. Geophys. Res.*, **105**(A6), 12,907–12,917, doi:10.1029/2000JA900010.
- Meredith, N. R., R. Horne, and R. Anderson (2001), Substorm dependence of chorus amplitudes: Implications for the acceleration of electrons to relativistic energies, *J. Geophys. Res.*, **106**(A7), 13,165–13,178, doi:10.1029/2000JA900156.
- Meredith, N. P., M. Cain, R. B. Horne, R. M. Thorne, D. Summers, and R. R. Anderson (2003), Evidence for chorus-driven electron acceleration to relativistic energies from a survey of geomagnetically disturbed periods, *J. Geophys. Res.*, **108**(A6), 1248, doi:10.1029/2002JA009764.
- Meredith, N. P., R. B. Horne, R. M. Thorne, and R. R. Anderson (2009), Survey of upper band chorus and ECH waves: Implications for the diffuse aurora, *J. Geophys. Res.*, **114**, A07218, doi:10.1029/2009JA014230.
- Miyoshi, Y., Y. Katoh, T. Nishiyama, T. Sakanoi, K. Asamura, and M. Hirahara (2010), Time of flight analysis of pulsating aurora electrons, considering wave-particle interactions with propagating whistler mode waves, *J. Geophys. Res.*, **115**, A10312, doi:10.1029/2009JA015127.
- Newell, P. T., T. Sotirelis, and S. Wing (2009), Diffuse, monoenergetic, and broadband aurora: The global precipitation budget, *J. Geophys. Res.*, **114**, A09207, doi:10.1029/2009JA014326.
- Newell, P. T., T. Sotirelis, and S. Wing (2010), Seasonal variations in diffuse, monoenergetic, and broadband aurora, *J. Geophys. Res.*, **115**, A03216, doi:10.1029/2009JA014805.
- Ni, B., R. M. Thorne, Y. Y. Shprits, and J. Bortnik (2008), Resonant scattering of plasma sheet electrons by whistler-mode chorus: Contribution to diffuse auroral precipitation, *Geophys. Res. Lett.*, **35**, L11106, doi:10.1029/2008GL034032.
- Ni, B., R. M. Thorne, R. B. Horne, N. P. Meredith, Y. Y. Shprits, L. Chen, and W. Li (2011a), Resonant scattering of plasma sheet electrons leading to diffuse auroral precipitation: 1. Evaluation for electrostatic electron cyclotron harmonic waves, *J. Geophys. Res.*, **116**, A04218, doi:10.1029/2010JA016232.
- Ni, B., R. M. Thorne, N. P. Meredith, R. B. Horne, and Y. Y. Shprits (2011b), Resonant scattering of plasma sheet electrons leading to diffuse auroral precipitation: 2. Evaluation for whistler-mode chorus waves, *J. Geophys. Res.*, **116**, A04219, doi:10.1029/2010JA016233.
- Olson, W. P., and K. Pfitzer (1977), Magnetospheric magnetic field modeling, *Rep. F44620-75-c-0033*, Air Force Off. of Sci. Res., London.
- Orlova, K. G., and Y. Y. Shprits (2010), Dependence of pitch-angle scattering rates and loss timescales on the magnetic field model, *Geophys. Res. Lett.*, **37**, L05105, doi:10.1029/2009GL041639.
- Petrinec, S. M., D. L. Chenette, J. Mobilia, M. A. Rinaldi, and W. L. Imhof (1999), Statistical X-ray auroral emissions: PIXIE observations, *Geophys. Res. Lett.*, **26**(11), 1565–1568, doi:10.1029/1999GL900295.

- Roeder, J. L., and H. C. Koons (1989), A survey of electron cyclotron waves in the magnetosphere and the diffuse auroral electron precipitation, *J. Geophys. Res.*, 94(A3), 2529–2541, doi:10.1029/JA094iA03p02529.
- Sandford, B. P. (1968), Variations of auroral emissions with time, magnetic activity and the solar cycle, *J. Atmos. Terr. Phys.*, 30, 1921–1942, doi:10.1016/0021-9169(68)90001-9.
- Santolík, O., D. A. Gurnett, J. S. Pickett, J. Chum, and N. Cornilleau-Wehrlin (2009), Oblique propagation of whistler mode waves in the chorus source region, *J. Geophys. Res.*, 114, A00F03, doi:10.1029/2009JA014586.
- Schulz, M., and L. J. Lanzerotti (1974), *Particle Diffusion in the Radiation Belts*, Springer, New York.
- Shprits, Y. Y., and B. Ni (2009), Dependence of the quasi-linear scattering rates on the wave-normal distribution for chorus waves in the radiation belt, *J. Geophys. Res.*, 114, A11205, doi:10.1029/2009JA014223.
- Shprits, Y. Y., R. M. Thorne, R. B. Horne, and D. Summers (2006a), Bounce-averaged diffusion coefficients for field-aligned chorus waves, *J. Geophys. Res.*, 111, A10225, doi:10.1029/2006JA011725.
- Shprits, Y. Y., W. Li, and R. M. Thorne (2006b), Controlling effect of the pitch-angle scattering rates near the edge of the loss cone on electron lifetimes, *J. Geophys. Res.*, 111, A12206, doi:10.1029/2006JA011758.
- Su, Z., H. Zheng, and S. Wang (2009), Evolution of electron pitch-angle distribution due to interactions with whistler mode chorus following substorm injections, *J. Geophys. Res.*, 114, A08202, doi:10.1029/2009JA014269.
- Su, Z., H. Zheng, and S. Wang (2010), A parametric study on the diffuse auroral precipitation by resonant interaction with whistler mode chorus, *J. Geophys. Res.*, 115, A05219, doi:10.1029/2009JA014759.
- Summers, D. (2005), Quasi-linear diffusion coefficients for field-aligned electromagnetic waves with applications to the magnetosphere, *J. Geophys. Res.*, 110, A08213, doi:10.1029/2005JA011159.
- Summers, D., and B. Ni (2008), Effects of latitudinal distributions of particle density and wave power on cyclotron resonant diffusion rates of radiation belt electrons, *Earth Planets Space*, 60, 763–771.
- Summers, D., B. Ni, and N. P. Meredith (2007a), Timescales for radiation belt electron acceleration and loss due to resonant wave-particle interactions: 1. Theory, *J. Geophys. Res.*, 112, A04206, doi:10.1029/2006JA011801.
- Summers, D., B. Ni, and N. P. Meredith (2007b), Timescales for radiation belt electron acceleration and loss due to resonant wave-particle interactions: 2. Evaluation for VLF chorus, ELF hiss, and electromagnetic ion cyclotron waves, *J. Geophys. Res.*, 112, A04207, doi:10.1029/2006JA011993.
- Swift, D. W. (1981), Mechanisms for auroral precipitation: A review, *Rev. Geophys.*, 19(1), 185–211, doi:10.1029/RG019i001p00185.
- Tao, X., R. M. Thorne, W. Li, B. Ni, N. P. Meredith, and R. B. Horne (2011), Evolution of electron pitch-angle distributions following injection from the plasmasheet, *J. Geophys. Res.*, 116, A04229, doi:10.1029/2010JA016245.
- Thorne, R. M., and C. F. Kennel (1967), Quasi-trapped VLF propagation in the outer magnetosphere, *J. Geophys. Res.*, 72(3), 857–870, doi:10.1029/JZ072i003p00857.
- Thorne, R. M., T. P. O'Brien, Y. Y. Shprits, D. Summers, and R. B. Horne (2005), Timescale for MeV electron microburst loss during geomagnetic storms, *J. Geophys. Res.*, 110, A09202, doi:10.1029/2004JA010882.
- Thorne, R. M., B. Ni, X. Tao, R. B. Horne, and N. P. Meredith (2010), Scattering by chorus waves as the dominant cause of diffuse auroral precipitation, *Nature*, 467, 943–946, doi:10.1038/nature09467.
- Tsyganenko, N. A. (1989), A magnetospheric magnetic field model with a warped tail current sheet, *Planet. Space Sci.*, 37, 5–20, doi:10.1016/0032-0633(89)90066-4.
- Tsyganenko, N. A. (2002), A model of the near magnetosphere with a dawn-dusk asymmetry: 1. Mathematical structure, *J. Geophys. Res.*, 107(A8), 1179, doi:10.1029/2001JA000219.
- Tsyganenko, N. A., and D. P. Stern (1996), Modeling the global magnetic field of the large-scale Birkeland current systems, *J. Geophys. Res.*, 101(A12), 27,187–27,198, doi:10.1029/96JA02735.
- Tsyganenko, N. A., H. J. Singer, and J. C. Kasper (2003), Storm-time distortion of the inner magnetosphere: How severe can it get?, *J. Geophys. Res.*, 108(A5), 1209, doi:10.1029/2002JA009808.
- Villalón, E., and W. J. Burke (1995), Pitch-angle scattering of diffuse auroral electrons by whistler mode waves, *J. Geophys. Res.*, 100(A10), 19,361–19,369, doi:10.1029/95JA01161.
- Wolf, R. A., R. W. Spiro, and F. J. Rich (1991), Extension of convection modeling into the high-latitude ionosphere: Some theoretical difficulties, *J. Atmos. Terr. Phys.*, 53(9), 817–829, doi:10.1016/0021-9169(91)90096-P.
- Wrenn, G. L., J. F. E. Johnson, and J. J. Sojka (1979), Stable “pancake” distributions of low energy electrons in the plasma trough, *Nature*, 279, 512–514, doi:10.1038/279512a0.
- Young, T. S. T., J. D. Callen, and J. E. McCune (1973), High-frequency electrostatic waves in the magnetosphere, *J. Geophys. Res.*, 78(7), 1082–1099, doi:10.1029/JA078i007p01082.

N. P. Meredith, British Antarctic Survey, Natural Environment Research Council, High Cross, Madingley Road, Cambridge CB3 0ET, UK.

B. Ni, K. G. Orlova, Y. Y. Shprits, and R. M. Thorne, Department of Atmospheric and Oceanic Sciences, University of California, Los Angeles, CA 90095, USA. (bbni@atmos.ucla.edu)